Functionalization using biocompatible carboxylated cyclodextrins of iron-based nanoMIL-100

Thais Carmona,[a,b] José F. Marco,[d] Mónica Giménez-Marqués,[e] Walter Cañón-Mancisidor,[b,f] Marlen Gutiérrez-Cutiño,[a,b] Patricio Hermosilla-Ibáñez,[a,b] Edwin G. Pérez,[c] Guillermo Mínguez Espallargas,[e] Diego Venegas-Yazigi*[a,b]

a Dr. T. Carmona, Dr. M. Gutiérrez-Cutiño, Dr. P. Hermosilla-Ibáñez, Prof. Dr. Diego Venegas-Yazigi
Materials Chemistry Department
Faculty of Chemistry and Biology, University of Santiago of Chile (USACH)
Av. Libertador Bdo. O´Higgins 3363, 9170022, Santiago de Chile, Chile

b Dr. T. Carmona, Dr. W. Cañón-Mancisidor, Dr. M. Gutiérrez-Cutiño, Dr. P. Hermosilla-Ibáñez, Prof. Dr. Diego Venegas-Yazigi
Center for the Development of Nanoscience and Nanotechnology (CEDENNA)
University of Santiago of Chile (USACH)
Av. Libertador Bdo. O´Higgins 3363, 9170022, Santiago de Chile, Chile
E-mail: diego.venegas@usach.cl

c Prof. Dr. E. G. Pérez
Departamento de Química Orgánica
Facultad de Química y de Farmacia
Pontificia Universidad Católica de Chile
Av. Vicuña Mackenna 4860, Santiago de Chile, Chile

d Dr. J. F. Marco
Instituto de Química Física “Rocasolano”
Consejo Superior de Investigaciones Científicas (CSIC)
Serrano 119, 28006, Madrid, Spain

e Dr. M. Giménez-Marqués, Dr. G. Mínguez Espallargas
Instituto de Ciencia Molecular (ICMol)
Universitat de València
Catedrático José Beltrán Martínez 2, 46980, Paterna, Spain

f Dr. W. Cañón-Mancisidor
Mathematical and Engineering Sciences Department
Faculty of Engineering, Sciences and Technology, University Bernardo O`Higgins (UBO)
Av. Viel 1497, 8370993, Santiago de Chile, Chile

Abstract: Here we report the first example of nanoMIL-100 particles modified with monomeric cyclodextrin derivatives of different length by exploiting strong interactions between non-saturated iron trimers at the external surface and carboxylate functionalities located at the end of biocompatible and flexible linkers of cyclodextrins. The main results revealed that, after the functionalization, the cyclodextrins are selectively located at the external surfaces covering the nanoparticles. Z potential measurements show that this functionalization induced changes respect to the bare nanoMIL-100 particles, however, the presence of the cyclodextrins does not modify the size neither porosity of the nanoparticles. The amount of cyclodextrins attached, investigated by thermogravimetry, increases with the length of the linker between CD cavity and nanoparticle surface, reaching up a 9 % wt. Auger spectroscopy suggested a clear predominant sp^3 character after the functionalizations (*vs*. sp^2 predominance in the unmodified nanoMIL-100). This study supposes the creation of an alternative family of hybrids based on carboxylated monomeric cyclodextrins.

Keywords: Surface modified nanoparticles, Cyclodextrins, Metal-organic frameworks, Cyclodextrin applications

*: Corresponding Author: E-mail: diego.venegas@usach.cl

Tel: +56 227181079

1. Introduction

Metal–Organic Frameworks (MOFs) are a family of porous crystalline self-assembled materials form by polydentate ligands that coordinated to metal clusters [1].It is possible to tailor the properties of MOFs. For instance, by the selection of the metal nodes and the ligands, the porosity, size, flexibility, topology or structure can be tuned leading to a highly versatile family of materials. MOFs can be exploited in numerous applications, including traditional storage [2, 3], separation and catalysis [4, 5], and in newer areas such as sensors [6], renewable energy [7], functional membranes [8], or medicine [9-15]. In recent years, MOFs fabricated using transition metal

ions and polycarboxylates have been emerged as an important class of materials suitable for such bio-applications [16-22].

Particularly, iron-based MOFs, especially iron (III) trimesate (MIL-100(Fe)), built from the assembly of oxo-centred trimers seem a perfect choice to be used for biomedical applications since it is possible to thoroughly achieve the control of the size by downsizing to the nanoscale regime (nanoMIL-100) [17, 21, 23, 24]. Also, the nanoMIL-100 presents large accessible and permanent porosity with large (29 Å) and small (24 Å) mesoporous cages, good biodegradability, high drug loading capacities [9, 25-29] and tolerance to *in vivo* conditions [30-32].

A key aspect for the use of nanoMOFs in the biomedical field relies on the fine control of the interaction between the exposed nanoMOF surface and the surrounding media. This often hampers their effective application due to the nanoparticles underwent a fast aggregation process in most common physiological media [31]. One rational approach to avoid this problem is to functionalize the outer surface with organic molecules or polymers that efficiently protect the nanoparticles against aggregation without altering its structural integrity and porosity. Thus, a variety of functional polymers have been investigated to coat MIL-100(Fe) such as silica [33], sodium alginate [34], phospholipids [35], polyethylenglycol [36], chitosan [37], heparin [38], or comb-like dextran copolymers [39], among others. The ample functionalization explored in MIL-100 is mainly due to the presence of non-saturated metal sites that provide opportunities to bind to MIL100 nanoparticles, through strong covalent interactions between the exposed trimer sites at the external surfaces and iono-groups (i.e. carboxylate, sulphate, phosphate, among others)

Among the possible coating agents used so far, cyclodextrins (CDs) result particularly interesting. These molecular entities made of 6, 7, or 8 α-1,4 linked glucose units, named as α-, β-, and γ-CD, respectively, have been largely used as functional coatings for drug delivery units due to their biocompatibility, hydrophilicity and chemical versatility, affording the plausible incorporation of new functionalities 'on-demand' that permits the design of new CD derivatives with interesting properties [40]. Moreover, CDs result particularly convenient for selectively decorating the outer surface of the porous structures such as MIL-100(Fe) MOF, taking into account that the section of the beta CDs is larger than the accessible MOF windows (~5.5 and ~8.4 Å) [41]. In particular, modified monomeric CDs derivatives have been used to coat iron trimesate nanoMOFs [42-44] without changing the porosity and crystallinity of the MOF, mainly by covalent linkage between phosphate groups directly anchored to the rings of the CDs and the non-saturated iron trimer sites on the surface of nanoparticles, achieving optimal functionalization degrees in a simple and fast and biocompatible method. However, is known that Fe-based nanoMOFs degrade progressively in the presence of phosphate ions due to the coordination to their "free" iron sites when are exposed to biological media conducting to an uncontrolled drug release [45, 46], limiting their applications for controlled drug delivery devices. Inspired by the nature of the MOF formed by carboxylate organic linkers, the creation of cyclodextrin derivatives with the presence of this functional group that permits strong interactions with the available non-saturated iron trimer of the nanoMOF sites is logical. This approach has been much less exploited. Up to date only a core–shell nanocomposite based on γ-CD oligomers with carboxylate anchoring groups has been studied using nanoMIL-100 particles as core material reaching up to 53 ± 8.4 wt% of oligomers associated to the nanoMOFs [47].

Here, we describe the synthesis of a hybrid material based on the functionalization of iron-trimesate MIL-100 nanoMOF (NanoMIL-100(Fe)) with monomeric carboxylate-ended cyclodextrin derivatives. In particular, biocompatible new cyclodextrin derivatives bearing carboxylate terminal groups have been obtained upon insertion of functionalities based on natural products such as succinyl and glutaryl moieties. Physicochemical characterizations have been performed by a set of complementary techniques such as FTIR, XRPD, TGA, N_2 adsorption measurements, SEM, TEM, DLS and XPS that have permitted the determination of the successful synthesis of the hybrids and the location of the organic functional coating. Information of changes in the environment of the external iron trimers and analytical information of the Csp^2:Csp^3 ratio on the surfaces of the new hybrids have been obtained by Mössbauer and X-ray induced Auger spectroscopies, respectively.

2. Experimental Section

2.1 General

In this work reagents (AK Scientific with exception of Iron (III) chloride hexahydrate (Scharlau)) and solvents (Sigma or Merck) were commercial and used without further purification. All aqueous procedures used ultrapure water obtained from a Millipore Milli-QPlus system (Millipore SpA, Milan, Italy).

2.2 Synthesis and activation of nanoMIL-100

Microwave assisted hydrothermal synthesis (Anton Paar, Monowave400, Power maximum output 850 W) on a 30 mL vessel were placed Iron (III) chloride hexahydrate (2.43 g, 9.00 mmol) and trimesic acid (0.84 g, 4.00 mmol) in 20 mL of distilled water. The mixture was heated to 130 °C over 30 s, then maintained at this temperature for 5 min 30 s and, finally cooled to 70 °C. The vessel was placed in an ice bath for 15 min. Nanoparticles were collected by centrifugation at 7500 rpm for 20 minutes at 25 °C. Washing was carried out 4 times with 20 mL water and 4 times with 20 mL absolute ethanol; each time using a vortex to re-disperse and centrifugation to collect. An orange solid was thus recovered which was stirred 1.75 h in a solution of KF (0.1 M), then centrifugated and washed twice with 20 mL of water and 20 mL of ethanol.

2.3 Synthesis and characterization of the cyclodextrin derivatives

2.3.1 Preparation of 6-monodeoxy-monotosyl-β-cyclodextrin (1)

11.60 g of β-cyclodextrin was suspended in 90 mL of water in a 250 mL round bottom flask. 34 mL of a solution of NaOH 3M was added dropwise within 1/2 h. The clear solution was stirred for additional 15 min. Then, 2.52 g (1.5 eq.) of p-toluensulfonyl chloride (pTsCl) was added in 5 portions at 5 min intervals. After the addition of the last portion the reaction mixture was stirred 1 h at room temperature and filtered off to eliminate the excess of non-reacting pTsCl. The solution was transferred to a 500 mL round bottom flask and 9.50 g of NH_4Cl was added. Immediately a white precipitated appeared. The solvent was partially eliminated till 2/3 of the initial volume. The mixture was cooled overnight, the white precipitate was filtered off and washed with 2 portions of 20 mL of cold water and 20 mL of cold MeOH and dried 12 h at 60 °C. 2.9 g were obtained (25 % yield) ^{1}H-NMR (400 MHz, DMSO- d6, δ): 7.75 (d, ^3J=8.3 Hz, 2H, H_a), 7.43 (d, ^3J=8.4 Hz, 2H, H_b), 5.83 – 5.61 (m, 14H, OH2+OH3), 4.88 – 4.73 (m, 7H, H1), 4.55 – 4.39 (m, 6H, OH6), 4.37 – 4.29 (m, 2H, H6´), 4.24 – 4.14 (m, 1H, $H_{5'}$), 3.76 – 3.44 (m, 25H, H_3+H_5+H_6), 3.43 – 3.17 (overlapping with HDO, m, 14H, H_2+H_4), 2.43 (s, 3H, -CH_3). ^{13}C-NMR (101 MHz, DMSO- d6, δ): 145.3(C_d), 133.1(C_e), 130.4(C_b), 128.0(C_a), 102.4(C_1 of βCD), 101.7($C_{1'}$ of βCD) 82.0($C_{4'}$ of βCD), 81.2(C_4 of βCD), 73.5(C_2 of βCD), 73.2($C_{3'}$ of βCD), 72.9(C_3 of βCD), 72.5(C_5 of βCD), 70.2($C_{5'}$ of βCD), 69.4($C_{6'}$ of βCD), 60.4(C_6 of βCD), 21.7(C_c). FTIR (ATR): 3292 (-OH) 2927 (C-H_{str}), 1637, 1542, 1489 (C-$C_{arom,\ str}$), 1158 (O-S-O_{str}), 1024 (i, C-O-C_{str}) cm-1. ESI-MS (m/z): calculated for $C_{49}H_{76}O_{37}S$, 1288.4; found, 1311.4 for $[M+Na]^+$.

2.3.2 Preparation of 6-monodeoxy-6-monoazido-β-cyclodextrin (*2*)

10.57 g (8.20 mmol) of **1** and 2.64 g (40.61 mmol, 5 eq.) of NaN_3 were dissolved in 50 mL of dry DMF in a 100 mL round bottom flask. The solution was heated to 80 °C 24 h. Then was cooled down to room temperature and precipitated with acetone. The mixture was stirred at 80 °C for 24 h, precipitated in acetone, and filtered. The crude product was recrystallized by dissolving it in hot water and precipitating in acetone. This procedure was repeated until FTIR showed no peak from residual sodium azide (at 2138 cm^{-1}) was observed. There was obtained. 5.8 g of a white powder (60 %). ^{1}H-NMR (400 MHz, DMSO-d_6, δ): 5.8 – 5.6 (m, 14H, OH_2+OH_3), 4.9 – 4.7 (m, 7H, H_1), 4.6 – 4.4 (m, 6H, OH_6), 3.8 – 3.5 (m, 28H, H_3+H_5+H_6), 3.42 – 3.23 (overlapping with HDO, m, 14H, H_2+H_4). ^{13}C-NMR (101 MHz, DMSO- d_6, δ): 101.9(C_1 of βCD), 101.6($C_{1'}$ of βCD), 83.5($C_{4'}$ of βCD), 81.5(C_4 of βCD), 73.1(C_2 of βCD), 72.4($C_{3'}$ of βCD), 72.2(C_5 of βCD), 72.0(C_3 of βCD), 70.2($C_{5'}$ of βCD), 59.9(C_6 of βCD), 51.6($C_{6'}$ of βCD). FTIR (ATR): 3383 (-OH), 2918 (C_{sp3}-H_{str}), 2101 (-$N_{3,str}$), 1024 (C-O-C_{str}) cm^{-1}. ESI-MS (m/z): calculated for $C_{42}H_{69}O_{34}N_3$, 1160.0; found, 1182.5 for $[M+Na]^+$.

2.3.3 Preparation of 6-monodeoxy-6-monoamino-β-cyclodextrin (3)

2.50 g (2.11 mmol) of **2** in 5 ml of dry DMF and 0.61 g (2.32 mmol, 1.1 eq.) of triphenylphosphine were placed in a 10 mL round bottom flask. The system was sealed under N_2. This solution was stirred 2 hours under the protection of the N_2 atmosphere at room temperature. Then was open to the atmosphere and 435 µL of water were added. The solution was heated to 90 °C for 3 hours. Cool down to room temperature and precipitated with acetone. The precipitate was washed with two portions of 20 mL of acetone and dried at 60 °C 12 hours. 2.24 g of a white powder (93 % yield) were obtained. ^{1}H-NMR (400 MHz, DMSO-d_6): 5.88 – 5.56 (m, 14H, OH_2+OH_3), 4.91 – 4.77 (m, 7H, H_1), 4.57 – 4.32 (m, 6H, OH_6), 3.95 – 3.46 (m, 28H, H_3+H_5+H_6), 3.43–3.23 (overlap with HDO, m, 16H, H_2+H_4+NH_2). ^{13}C-NMR (101 MHz, DMSO-d_6, δ): 101.9(C_1 of βCD), 81.6(C_4 of βCD), 81.5(C_2 of βCD), 73.1(C_5 of βCD), 72.4(C_3 of βCD), 72.0(C_6 of βCD), 59.9(C_6 of βCD), 41.9($C_{6'}$ of βCD). FTIR (ATR): 3428 (-OH), 2928 (C_{sp3}-H_{str}), 1029 (C-O-C_{str}). cm^{-1}. ESI-MS (m/z): calculated for $C_{42}H_{71}O_{34}N$, 1134.3; found, 1135.5.

2.3.4 Preparation of 6-monodeoxy-6-amidosuccinyl-β-cyclodextrin (4)

To 501 mg (0.44 mmol) of **3** dissolved in 12 mL of dry DMF were added 58.5 mg (0.58 mmol, 1.1 eq.) of succinic anhydride dissolved in 2 mL of DMF with vigorous stirring. After 3h of stirring at room temperature the solvent was evaporated. The viscous residue was precipitated with 100 mL of acetone and filtered off. The white precipitate was dissolved in 5 mL of water, stirred 30 mins and reprecipitated in acetone, filtered and dried 12 h at 60 °C. 447 mg (82% yield) of the title compound were obtained. ^{1}H-NMR (400 MHz, D_2O, δ): 5.15 – 5.06 (m, 7H, H_1), 4.06 – 3.84 (m, 28H, H_2+H_3+H_4+H_5), 3.71 – 3.59 (m, 12H, H_6), 3.46 (d, 1H, ^3J=9.0 Hz, $H_{6'}$), 3.32 (dd, 1H, ^3J=14.7, 8.5 Hz, $H_{6''}$), 2.64 – 2.51 (m, 4H, -$(CH_2)_2$-). ^{13}C NMR (101 MHz, D_2O, δ): 177.4(COOH), 174.9(CONH), 101.9(C_1 of βCD), 101.5($C_{1'}$ of βCD) 83.1($C_{4'}$ of βCD), 81.1(C_4 of βCD), 73.1(C_2 of βCD), 72.0(C_3 of βCD), 71.7(C_5 of βCD), 70.6($C_{5'}$ of βCD), 60.2 (C_6 of βCD), 40.2($C_{6'}$ of βCD), 30.5(-CH_2-COOH), 29.9(-CH_2-CONH-). FTIR (ATR): 3430 (-OH), 2920 (C_{sp3}-H_{str}), 1024 (C O-C_{str}) cm^{-1}. ESI-MS (m/z): calculated for $C_{46}H_{75}NO_{37}$, 1233.4; found, 1255.6 for $[M+Na]^+$

2.3.5 Preparation of 6-monodeoxy-6-amidoglutaryl-β-cyclodextrin (5)

To 505 mg (0.44 mmol) of **3** dissolved in 12 mL of dry DMF were added under the protection of inert atmosphere 66.3 mg (0.58 mmol, 1.3 eq.) of glutaric anhydride dissolved in 1 mL of DMF under vigorous stirring: This mixture was stirred 2.5 hours at room temperature. Then was precipitated with 50 mL of ethyl acetate stirred 1 hour and filtered off. The white precipitate was dissolved in 5 mL water and stirred 30

minutes, reprecipitated in acetone and filtered. After drying 12 hours at 60 °C 355 mg of the title compound was obtained (64 % yield). ^{1}H-NMR (400 MHz, D_2O, δ): 5.10 – 5.02 (m, 7H, H_1), 4.07 – 3.80 (m, 28H, H_2+H_3+H_4+H_5), 3.73 – 3.57 (m, 12H, H_6) 3.46 (t, ^{3}J=9.2 Hz, 1H, $H_{6}^{'}$), 3.32 (dd, ^{3}J=14.8, 8.7 Hz, 1H, $H_{6}^{''}$), 2.48 – 2.32 (m, 4 H, -CH_2-C=O-NH- and -CH_2-COOH), 2.00 – 1.83 (m, 2H, -CH_2-). FTIR (ATR): 3430 (-OH_{str}), 2920 (C_{sp3}-H_{str}), 1024 (C O-C_{str}) cm^{-1}. ^{13}C NMR (101 MHz, D_2O, δ): 178.1(C=O), 175.4(C=O), 101.9(C_1 of βCD), 83.2(C_1 of βCD), 81.1(C_1 of βCD), 81.0(C_1 of βCD), 80.8(C_1 of βCD), 73.1(C_1 of βCD), 72.0(C_1 of βCD), 71.7(C_1 of βCD), 70.4(C_1 of βCD), 60.2(-CH_2-OH of βCD), 40.2(-CH_2-NH of βCD), 34.7(-CH_2-COOH), 29.7(-CH_2-CONH-), 20.8(-CH_2-). ESI-MS (m/z): calculated for $C_{47}H_{77}NO_{37}$, 1247.5; found, 1270.9 for $[M+Na]^+$.

2.4 Characterizations

The ^{1}H (^{13}C) Nuclear Magnetic Resonance (NMR) spectra were recorded NMR spectra were recorded on a Bruker Advanced 400 MHz spectrometer at 400 (100.6) MHz. at 300 K. Chemical shifts (δ)are given in parts per million (ppm) and referenced to the solvent residual signal. *J* values are given in Hertz (Hz).Fourier Transform Infrared Spectroscopy (FTIR) analyses were performed using a Jasco FTIR-4600 spectrophotometer equipped with an ATR accessory. Spectra were recorded in the 4000-400 cm^{-1} range at room temperature. Electrospray ionization mass spectrometry (ESI-MS) studies were done with a LTQ XL Linear Ion Trap Mass Spectrometer with the spray voltage set at 3 kV. Detection was performed in full scan mode in the 100–2000 m/z range in positive mode. The crystallinity and purity of MIL-100(Fe) nanoMOFs were assessed by X-ray powder diffraction (XRPD). Patterns were collected in a Bruker D8 Advance with Lyxneye detector and variable optical or PANalytical Empyrean X-ray platform with PIXcel detector with capillary powder diffraction (transmission mode measurement) set up using Cu radiation (Kα1, λ= 1.5406 Å) from 2 to 30º (2θ) a step size of 0.02º and 4° per step in continuous mode. The nanoparticle size was measured with a Malvern Zetasizer (Malvern, UK). 100 µg/ml dispersions of the modified and unmodified nanomaterials were prepared in fresh MilliQ water and sonicated for 15 mins. The measurements were performed in polystyrene cells within an hour after the dispersion procedure. Images were obtained from Zeiss model Evo MA10 equipped with Tungsten with an acceleration voltage of 20 kV and 8 mm of working distance. For the Transmission Electron Microscopy (TEM) drops of sample (~2 mg/ml) were dropped on a copper grid and air-dried. The samples were examined by a Hitachi HT7700 microscope operating at an accelerating voltage of 120.0 keV. Average sizes were determined by measuring diameters along a consistent axis throughout the samples.Analyses were carried out between 25 and 600(800) ºC with a heating rate of 10 ºCmin^{-1} under air conditions using a TGA/DSC Mettler Toledo.

2.4.9 X-Ray Photoelectron Spectroscopy (XPS). Data were recorded with a SPECS-150 hemispherical electron analyzer at a take-off angle of 90º, using Mg Kα radiation (1253.6 eV) and a constant pass energy of 20 eV, under a base pressure lower than $2{\cdot}10^{-9}$ mbar. The XPS source was operated at a power of 100 W instead of the most usual 300 W to minimize the possible radiation damage of the organic samples. The binding energy scale was referenced to the C-H/C-C peak which was set at 284.6 eV. All the spectra were fitted with the CasaXPS software using a sum of pseudo Voight line profiles (70% Gaussian-30% Lorentzian) and a Shirley background. ^{57}Fe Mössbauer transmission spectra were recorded at room temperature using a constant acceleration spectrometer with a ^{57}Co(Rh) source. Absorbers were prepared to contain *ca.* 5 mg/cm^2 of natural iron. The velocity scale was calibrated using an α-Fe foil 6 µm thick. All the spectra were computer-fitted and the isomer shift values were referred to the centroid of the α-Fe sextet at room temperature. Adsorption isotherms of N_2 were measured at 77 K in an IGA-100 gravimetric gas sorption analyzer (Hiden Isochema) using approximately 50 mg of sample. The sample was outgassed at 398 K under vacuum for 3 hours.

3. Results and Discussion

3.1 Synthesis of nanoMIL-100 and surface modification with carboxylic CD derivatives

We carried out the synthesis of carboxylate functionalized β-CD derivatives for their use as functionalizing agents in the post synthetic surface modification of the iron-trimesate MIL-100 nanoMOF by adjusting methods previously reported [48-50]. (see Supporting Information for more details) The used synthetic route provided pure CD compounds avoiding the formation of undesired CD monomer/dimer mixtures which would be very difficult to separate by column chromatography techniques.

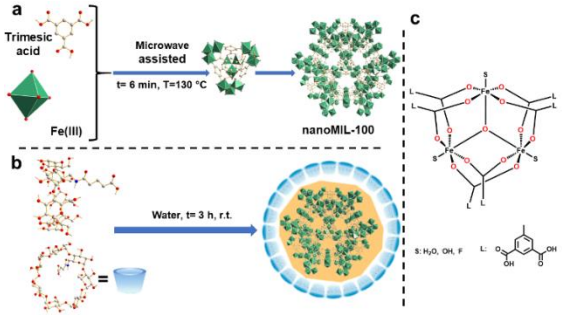

Scheme 1: a) Schematic representation of the synthesis of nanoMIL-100; b) Frontal and lateral view of the 6-monodeoxy-6-amidoglutaryl-β-cyclodextrin (**5**) and functionalization of the nanoMIL-100 with **5**.c) Schematic diagram of the coordination environment of the Fe-trimer SBU.

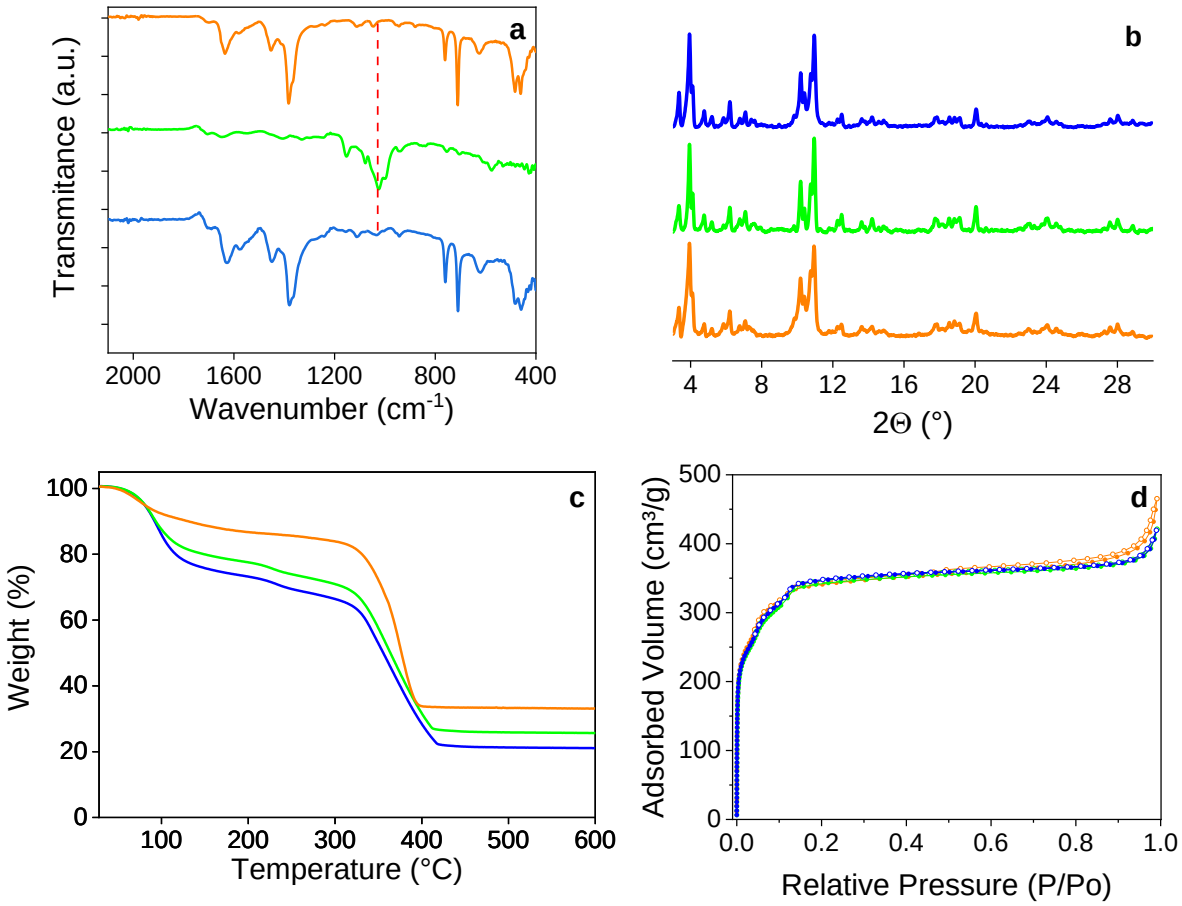

Figure 1. (a) FTIR spectra in the 2100 to 400 cm^{-1} range of the unmodified (—) and modified nanoMIL-100 cyclodextrin derivative **4** (—) and the hybrid material (—); (b) XRPD normalized patterns of nanoMIL-100 modified with **4** (—), **5** (—) and unmodified (—); (c) TGA analysis of nanoMIL100(Fe) (—) and after modification with cyclodextrin derivative **4** (—) and **5**(—); (d) N_2 adsorption-desorption isotherms of the unmodified nanoMIL-100 (—) and modified with **4** (—) and **5** (—).

NanoMIL-100 particles were synthesized by microwave assisted hydrothermal synthesis as previously described and stored wet [23]. Structure analysis of the obtained nanoMIL-100 by XRPD confirms that the polycrystalline sample corresponds with the previously reported Fe-trimesate MIL-100 material, with a particle measured size of 89 ± 33 and BET surface area of 1,245 m^2g^{-1} (see Supporting Information Fig. 1S for more details).

External surface functionalization of MIL-100 nanoparticles (2.5 mg, dried based) was directly performed by soaking the wet nanoparticles in CD derivatives **4** or **5** aqueous solutions (3.0 $mg{\cdot}mL^{-1}$, 1 mL) with orbital agitation for 3 h at room temperature. After stirring, nanoparticles were recovered by centrifugation (15 min at 15k rpm) and washed twice with water (1 mL each) to remove the excess of CD derivatives not linked to the surface of the nanoparticles.

The successful modification was first determined by FTIR, XRPD, TGA and N_2 adsorption measurements. FTIR spectra of the unmodified nanoMIL-100 and the nanomaterial obtained after functionalization with CD **4** are shown in Fig. 1a. In particular, the characteristic intense bands associated to the asymmetric and symmetric vibrational bands of the coordinated carboxylate groups in the nanoMIL-100 and the in-plane asymmetric stretch band, ν_{as} (Fe_3O), assigned to the iron oxocluster core [51], appeared at 1575, 1380 and 621 cm^{-1} respectively in the hybrid nanoparticles. These bands were unaffected after the coordination of the carboxylate groups of the cyclodextrins on the non-saturated sites of the iron trimers in the modified materials. In addition to the nanoMIL-100 associated bands, a low intense band appeared at ~1030 cm^{-1}, which are attributed to the C-O-C skeletal vibrations from the CDs and therefore confirm their presence in the new material. Similar vibrations have been observed by other authors when they performed post synthetic functionalizations using both native and modified cyclodextrins [33, 52-54]. Unfortunately, the amide band from the CD derivative could not be detected due to the overlapping of this band with the nanoMIL-100 carboxylate bands.

Fig. 1b shows the XRPD patterns before and after the modification process with CDs **4** and **5**, respectively. The

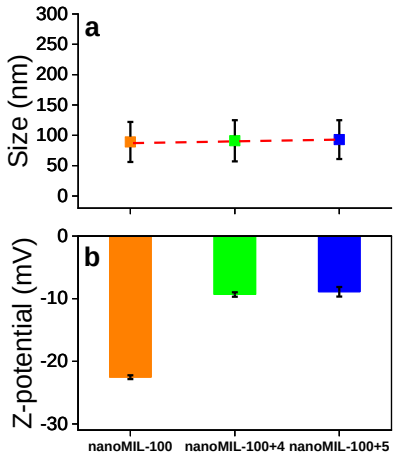

Figure 2. (a) Mean particle size obtained from TEM measurements; (b) Zeta potential of the unfunctionalized nanoMIL-100 (orange), functionalized with cyclodextrins **4** (green) and **5** (blue).

reflections presented in the unmodified nanomaterial were conserved in the treated ones, showing that the integrity of the lattice was preserved in the new hybrid nanomaterials [42, 43]. TEM micrographs obtained before and after functionalization with **4** and **5** revealed that no morphological differences were found the new hybrids respect to unmodified material (Figs. S10-S12, of the Supporting Information). The thermograms for the modified and unmodified materials under an air atmosphere are presented in Fig. 1c (for cyclodextrins **4** and **5** see Fig. S8 in Supporting Information). For the modified nanomaterials, a similar two-mass loss event profile was registered with two main differences respect to the uncoated nanoMIL-100. It was observed a broadening of the second mass loss to higher temperatures accompanied with an increased weight loss. The latter indicates the presence of additional organic components which combustion occurred at the same time as the trimesic acid from nanoMIL-100 on the modified nanomaterials until the total collapse of the framework. These additional weigh losses should be associated to the presence of the cyclodextrin derivatives. The amount of CDs anchored to the surface of the nanoparticles was determined by TGA analysis. Direct comparison of the inorganic residues in the dried unmodified and modified nanoparticles revealed a 5 and a 9 wt% of CD derivatives **4** and **5** respectively linked in the new hybrid nanomaterials. The latter value is slightly lower than the results obtained by Agostoni *et al.*[43] in which a 14 wt% was obtained after 1 h of incubation of monomeric CD-phosphate derivatives and in range with the results obtained by Cutrone *et al.*[44] with the CD-P decorated with mannose moieties directly attached or at the end of relatively short and flexible linkages at the primary faces. The different association to nanoMIL-100 observed when comparing CD derivatives **4** and **5** could be associated to the presence of an additional methylene group in CD **5** that avoids steric hindrance and therefore improves the association percentage. Fig. 1d shows the N_2 adsorption/desorption isotherms of the modified and unmodified nanoMIL-100 particles. After the modification, the calculated values were 1,226 and 1,238 for the new hybris the formed with CD **4** and **5**, respectively. (vs. 1245 m^2g^{-1} for the unmodified nanomaterial). The BET surface area after the functionalization was not affected by surface modification with CD derivatives suggesting that the CD derivatives should be located onto the nanoMIL-100 external surfaces as have been previously obtained [42, 43].

The size and changes at the external surfaces of the modified nanoparticles was investigated by TEM and DLS techniques. TEM analyses revealed (Fig. 2a) very close average diameters for the modified and unmodified nanoparticles, 91 ± 34 and 93 ± 32 for the modified nanoMIL-100 with **4** and **5** respectively *vs.* 89 ± 33 for the unmodified nanoMIL-100. (for statistical analysis see Figs. S10-S12). These results indicate that the mean size of the functionalized particles kept constant being lesser than 100 nm in both cases. Values below 100 nm have been obtained previously in dry state by different techniques [9, 35, 55, 56]. In the characterizations using DLS measurements, the estimated mean hydrodynamic diameter values were larger than the obtained using TEM, as expected, with moderate polidispersities (pdI > 0.3).

This can be explained by the tendency to agglomeration behaviour of the particles in solution. However, a striking difference were obtained when Z-potential values were measured. Results are depicted in Fig. 2b, which shows that the Z-potential values shifted from −22.5 mV for the unmodified nanoMIL-100 to values around a halve (~−10 mV) after the functionalization. The value before the modification indicates a dispersion with a rather good colloidal stability and a decrease of carboxylate pending groups substituted by F^- ions coordinated to the metallic centres of the framework which proportionate negative charges on the external surfaces of the nanoparticles as results of the activation process [57]. The variation of the Z-potential values towards less negative values can be associated to the substitution of the previously generated charges of those ions with the carboxylate moieties of the cyclodextrin derivatives. This supposes a decrease of the charge on the surface by a non-ionic cyclodextrin coverage leading to a decrease of the Z-potential values confirming the success of the functionalization.

3.2 Surface analysis of the functionalized nanoMIL-100 with cyclodextrin derivatives 4 and 5

XPS was used to ascertain the presence of the CD derivatives in the top layers (~5–10 nm depth) in the modified nanoMIL-100 particles. Fig. 3 shows the C1s core level spectra recorded from the unmodified nanoMIL-100, the free cyclodextrins **4** and **5** and the hybrid nanomaterials obtained after surface modification. The C1s XPS spectrum recorded from nanoMIL-100 was fitted to five different contributions (for further details see Supplementary Information). The main ones at 284.6 and 288.6 eV are characteristic “fingerprints” of

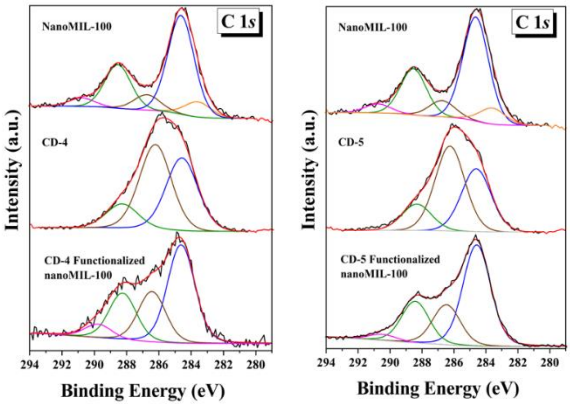

Figure 3. Left: C1s XPS spectra recorded from the unmodified nanoMIL-100, **4** and nanoMIL-100 functionalized with **4** (—); Right: C1s XPS spectra recorded from nanoMIL-100, **5** and nanoMIL-100 functionalized with **5**.

the carbon skeleton of the organic linker of nanoMIL-100 (C-C and C-OOH contributions, respectively) [43, 58].

The XPS spectra recorded from the synthesized cyclodextrins presented a C1s 'fingerprint' with a main contribution located at 286.3 eV associated to a C-O-C contribution, together with other components at 284.6 and 288.6 eV which, as mentioned above, can be assigned to the functional groups C-C and C-OOH, respectively. After the coating process, the C1s XPS profiles of the hybrid nanoparticles differ considerably of that of the uncoated material: an intense component located at 286.4 eV is now clearly observed. This should correspond to the presence of associated cyclodextrin derivatives, thus confirming the external surface location of the derivatives **4** and **5**. In fact, the C1s spectra recorded from the hybrid materials can be considered as a combination of the C1s spectra of the nanoMIL-100 material and those of the synthesized cyclodextrins These new contributions have been previously observed by Qiu *et al*.[47] when core–shell nanocomposite based on γ-CD oligomers with flexible bridges and carboxylate anchoring groups using nanoMIL-100 particles as core material has been studied. Overall, the XPS results confirm the successful coating with CDs of the nanoMIL-100 particles.

Table 1.- Hyperfine parameters and spectral areas obtained from the fit of the Mössbauer spectrum with no imposed restrictions

Site		nanoMIL100	5-coated	4-coated
1	δ (mms^{-1})	0.41	0.38	0.38
	Δ (mms^{-1})	0.20	0.16	0.14
	Area (%)	29	22	10
2	δ (mms^{-1})	0.43	0.41	0.44
	Δ (mms^{-1})	0.61	0.53	0.44
	Area (%)	48	47	44
3	δ (mms^{-1})	0.44	0.41	0.42
	Δ (mms^{-1})	1.05	0.96	0.87
	Area (%)	23	31	45

^{57}Fe Mössbauer spectroscopy can provide further insight into both the oxidation state and the environment of iron in the nanoMIL-100 samples. The Mössbauer spectra recorded from the unmodified nanoMIL-100 and from the modified materials with **4** and **5** are depicted in Fig. 6. They consist of an asymmetric quadrupole doublet with broadened lines.The corresponding Mössbauer parameters and spectral areas are collected in Table 1.

In all the cases, the isomer shifts and spectral areas are free parameters. The hyperfine parameters are characteristic of high spin Fe(III) ions in octahedral coordination. The presence of three different quadrupole doublets with quadrupole splittings ranging from 0.16 mms^{-1} to 1.05 mms^{-1} is indicative of the presence of, at least, three different octahedral environments, spanning from a quite symmetrical one (associated to the smallest quadrupole splitting) to a very distorted one (associated to the largest quadrupole splitting). It is quite plausible to associate the higher quadrupole splitting with those octahedra which contain F. In fact, as Table 1 indicates, in general terms the isomer shift is larger for the sites with higher quadrupole splittings with is indicative of a more marked ionic character of these particular iron species and, therefore, consistent with the presence of F as a ligand.

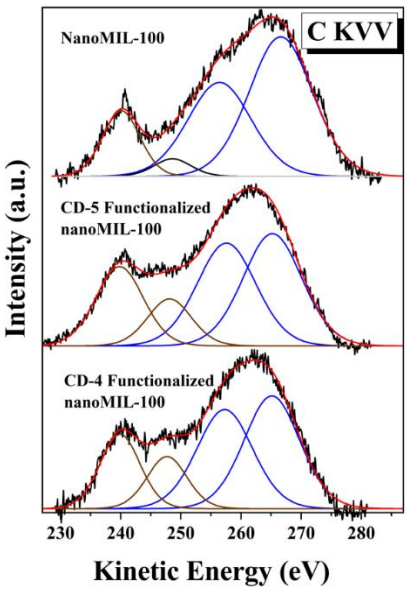

Figure 4. X-ray induced C KVV Auger spectra recorded from the unmodified nanoMIL-100 (top) and modified with CD **5** (middle) and **4** (bottom).

Li *et al.[46]* introduced a better approach to the evaluation of spectra such of these implies the use of quadrupole splitting (QS) distributions. As mentioned before, Table 1 suggests that the species with smaller quadrupole splitting has an isomer shift lower than those

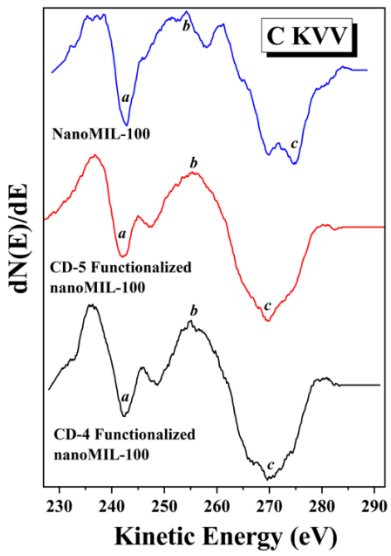

Figure 5. First derivative of the C KVV spectra depicted in Fig. 4.

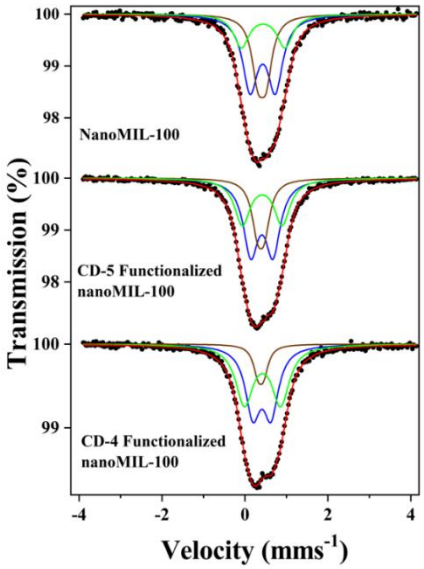

Figure 6. ^{57}Fe Mössbauer spectra recorded from the various samples fitted to three doublets with no restrictions imposed to their linewidths or their hyperfine parameters.

corresponding to the species with larger quadrupole splittings. Thus, in the fit we have introduced a small linear correlation between the isomer shifts and the quadrupole splittings in the distribution such that the isomer shift of the first doublet in the distribution is 0.38 mms^{-1} and that of the last doublet is 0.45 mms^{-1}. If this correlation is not contemplated, then a good fit cannot be obtained since a symmetrical QS distribution cannot match properly an asymmetric spectrum. Fig. 7 shows the results obtained from this type of fit.

The (QS) distribution corresponding to the unmodified nanoMIL-100 presents four well-defined maxima. The first three ones appear at Δ values similar to those collected in Tables 1 and S1, i.e., 0.14 mms^{-1}, 0.65 mms^{-1} and 1.08 mms^{-1} what indicates that the three-doublets discrete fit is a reasonable approach and, therefore, compatible with the existence of at least three main Fe(III) sites in octahedral coordination having different distortion degrees.

The fourth minor maximum at Δ=1.54 mms^{-1} is not an artefact as it appears consistently in the QS distributions of the three samples. In fact, a close look at the spectra indicates that this contribution tries to fit the small bump marked with an arrow in Fig. 7. This quadrupole splitting is really large and would correspond to a very distorted Fe(III) octahedral unit. Hence, this type of fit suggest the existence of four different Fe(III) environments in the material although the relative importance of the most distorted one is very small as it contributes with less than 5% to the total spectral area.

The distribution corresponding to the 5-coated material also presents four well-defined maxima although it shows a trend to become flatter than the previous one in the region 0.75-1.00 mms^{-1}. This trend is more general and accentuated in the distribution corresponding to the 4-coated sample as the second and third maxima are almost completely smeared out.

It is known[32] that the Mössbauer spectra are sensitive to changes in the environment of iron beyond its first coordination shell when its immediate coordination remains unchanged. This fact would imply the existence in this sample of a large multiplicity of octahedral species with different chemical environments beyond their first coordination sphere compatible with the occurrence of chemical disorder. In other words, functionalization of the nanoMIL-100 sample with **5** and **4** induces, especially in the case of the latter, a remarkable chemical disorder around the Fe(III) sites. This might be associated to changes in the environment surrounding the accessible iron trimers by the replacement of more labile molecules (*i.e* water, partially coordinated trimesate linkers) by the carboxylate terminal groups of the cyclodextrins. It could be expected that this chemical disorder can be particularly important near to the surface of the materials where a variety of situations which would include a different number of missing/substituting carboxylate terminal groups might occur.

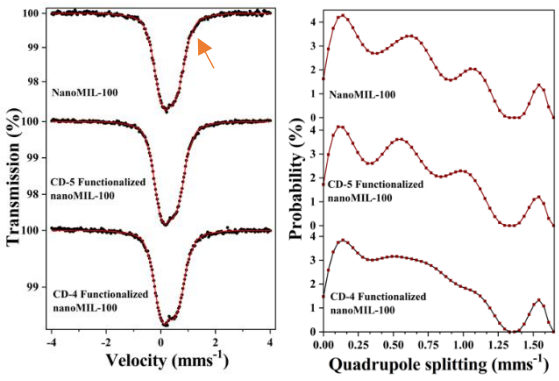

Figure 7. Left: ^{57}Fe Mössbauer spectra recorded from the various samples fitted to a quadrupole splitting distribution. Right: Corresponding quadrupole splitting distributions of the spectra on the left.

4. Conclusion

We report the synthesis of highly biocompatible β-CD modified with carboxylate-ended functionalities based on flexible linkers. These CD derivatives have been used for the external functionalization of porous nanoMIL-100 creating two new hybrids following a simple green and straightforward method. The successful synthesis of these new hybrid nanomaterials is evidenced by FTIR, XPS, Auger and TGA analysis. FTIR analysis of the new hybrids reveal the appearance of new bands associated to the cyclodextrins pointing out the presence of the cyclodextrins. XPS confirms the presence of cyclodextrin on the nanoparticles due to the presence of additional contributions in the spectra that are associated to the cyclodextrins. The crystalline porous structure was not disrupted upon CDs attachment, as the calculated BET surfaces after the coating process are unaffected indicating that the CDs derivatives are selectively located at the external surfaces. This efficient external selective functionalization is due by the section of the CD derivatives is larger than the accessible windows of the nanoMIL-100 preventing their entrance within the pores of the nanoparticles. TGA measurements show that CDs anchored reaching up to 9 wt% of coating associated to the nanoMOFs. Sizes measured by TEM afford diameters around 100 nm both for the uncoated and coated nanomaterials.

The presence of cyclodextrins at the external surfaces in the new hybrids is also supported by drastic changes in the sp^2:sp^3 ratio measured by X-ray Auger spectroscopy changing from almost 100 % of sp^2 hybridized carbons in the unmodified nanoMIL-100 to close to 100 % of sp^3 after the functionalization. By taking advantage on the inherently able to form inclusion complexes in water solution of cyclodextrins and the versatility of chemical modifications and the different hydrophobicity of their cavities than the nanoMIL-100 pores, this study paves the way for the construction of an alternative family of hybrids based on carboxylated monomeric CDs in which two drugs can be loaded in different compartments. Further studies about this potential application are currently in process in our laboratories.

Supporting Information

Synthesis and characterization of the nanoMIL-100, synthesis and characterization of the cyclodextrin derivatives **4** and **5** and characterization of the hybrids.

Author Contributions

T. Carmona: Conceptualization, Methodology, Investigation, Writing - original draft, Writing - review & editing. **W. Cañón-Mancisidor, M Gutierrez-Cutiño and P. Hermosilla-Ibañez:** Writing - review & editing Methodology, **E. G. Pérez, J. F. Marco , M. Gimenez-Marqués, G. Mínguez Espallargas**: Investigation, Writing - review & editing, **D. Venegas-Yazigi**: General supervision, Writing - review & editing.

Conflicts of interest

The authors declare that they have no known competing financial interests or personal relationships that could have appeared to influence the work reported in this paper.

Acknowledgements

Authors would like to thank to Center for the Development of Nanoscience and Nanotechnology CEDENNA AFB180001 basal project. TC would like to thank to Fondo Nacional para el Desarrollo Científico y Tecnológico (FONDECYT POSTDOCTORADO) proyect 3180454. Financial support from the Spanish Agencia Estatal de Investigación under project RTI2018-095303-B-C51 is gratefully acknowledged. This work was done under the LIA-M3-1027 CNRS Collaborative Program. The present work has been funded by 'Unidad de Excelencia María de Maeztu' MDM-2015-0538 granted to ICMol, and the Generalidad Valenciana (Prometeo/2019/076 program of excellence). M.G.M. acknowledges funding from the MINECO (Ramón y Cajal contract).

References

[1] N.R.C. Stuart R. Batten, Xiao-Ming Chen, Javier Garcia-Martinez, Susumu Kitagawa, Lars Öhrström, Michael O'Keeffe, Myunghyun Paik Suh and Jan Reedijk, Terminology of metal–organic frameworks and coordination polymers (IUPAC Recommendations 2013), Pure Appl. Chem., 85 (2013) 1715-1724.

[2] M. Eddaoudi, J. Kim, N. Rosi, D. Vodak, J. Wachter, M. O'Keeffe, O.M. Yaghi, Systematic Design of Pore Size and Functionality in Isoreticular MOFs and Their Application in Methane Storage, Science, 295 (2002) 469-472.

[3] E. Mahmoud, L. Ali, A. El Sayah, S.A. Alkhatib, H. Abdulsalam, M. Juma, A.H. Al-Muhtaseb, Implementing Metal-Organic Frameworks for Natural Gas Storage, Crystals, 9 (2019) 406-425.

[4] Q. Wang, D. Astruc, State of the Art and Prospects in Metal–Organic Framework (MOF)-Based and MOF-Derived Nanocatalysis, Chem. Rev. (Washington, D. C.), 120 (2020) 1438-1511.

[5] X.-Y. Dao, J.-H. Guo, X.-Y. Zhang, S.-Q. Wang, X.-M. Cheng, W.-Y. Sun, Structure-dependent iron-based metal–organic frameworks for selective CO2-to-CH4 photocatalytic reduction, J. Mater. Chem. A . 8 (2020) 25850-25856.

[6] W.P. Lustig, S. Mukherjee, N.D. Rudd, A.V. Desai, J. Li, S.K. Ghosh, Metal–organic frameworks: functional luminescent and photonic materials for sensing applications, Chem Soc Rev, 46 (2017) 3242-3285.

[7] H. Zhang, J. Nai, L. Yu, X.W. Lou, Metal-Organic-Framework-Based Materials as Platforms for Renewable Energy and Environmental Applications, Joule, 1 (2017) 77-107.

[8] X. Li, Y. Liu, J. Wang, J. Gascon, J. Li, B. Van der Bruggen, Metal–organic frameworks based membranes for liquid separation, Chem Soc Rev, 46 (2017) 7124-7144.

[9] P. Horcajada, T. Chalati, C. Serre, B. Gillet, C. Sebrie, T. Baati, J.F. Eubank, D. Heurtaux, P. Clayette, C. Kreuz, J.-S. Chang, Y.K. Hwang, V. Marsaud, P.-N. Bories, L. Cynober, S. Gil, G. Ferey, P. Couvreur, R. Gref, Porous metal-organic-framework nanoscale carriers as a potential platform for drug delivery and imaging, Nat Mater, 9 (2010) 172-178.

[10] C.-Y. Sun, C. Qin, X.-L. Wang, Z.-M. Su, Metal-organic frameworks as potential drug delivery systems, Expert Opin Drug Deliv, 10 (2013) 89-101.

[11] M. Giménez-Marqués, T. Hidalgo, C. Serre, P. Horcajada, Nanostructured metal–organic frameworks and their bio-related applications, Coord. Chem. Rev., 307 (2016) 342-360.

[12] M.A. Chowdhury, Metal-organic-frameworks for biomedical applications in drug delivery, and as MRI contrast agents, J. Biomed. Mater. Res. A, 105 (2017) 1184-1194.

[13] S. Rojas, A. Arenas-Vivo, P. Horcajada, Metal-organic frameworks: A novel platform for combined advanced therapies, Coord. Chem. Rev., 388 (2019) 202-226.

[14] J. Della Rocca, D. Liu, W. Lin, Nanoscale Metal–Organic Frameworks for Biomedical Imaging and Drug Delivery, Acc Chem Res, 44 (2011) 957-968.

[15] T. Simon-Yarza, S. Rojas, P. Horcajada, C. Serre, 4.38 The Situation of Metal-Organic Frameworks in Biomedicine☆, in: P. Ducheyne (Ed.) Comprehensive Biomaterials II, Elsevier, Oxford, 2017, pp. 719-749.

[16] K.M.L. Taylor, W.J. Rieter, W. Lin, Manganese-Based Nanoscale Metal−Organic Frameworks for Magnetic Resonance Imaging, J. Am. Chem. Soc., 130 (2008) 14358-14359.

[17] K.M.L. Taylor, A. Jin, W. Lin, Surfactant-Assisted Synthesis of Nanoscale Gadolinium Metal–Organic Frameworks for Potential Multimodal Imaging, Angew. Chem. Int. Ed., 47 (2008) 7722-7725.

[18] H. Zheng, Y. Zhang, L. Liu, W. Wan, P. Guo, A.M. Nyström, X. Zou, One-pot Synthesis of Metal–Organic Frameworks with Encapsulated Target Molecules and Their Applications for Controlled Drug Delivery, J Am Chem Soc, 138 (2016) 962-968.

[19] B. Yang, M. Shen, J. Liu, F. Ren, Post-Synthetic Modification Nanoscale Metal-Organic Frameworks for Targeted Drug Delivery in Cancer Cells, Pharm Res, 34 (2017) 2440-2450.

[20] A. Rengaraj, P. Puthiaraj, N.-S. Heo, H. Lee, S.K. Hwang, S. Kwon, W.-S. Ahn, Y.-S. Huh, Porous NH2-MIL-125 as an efficient nano-platform for drug delivery, imaging, and ROS therapy utilized Low-Intensity Visible light exposure system, Collid Surface B, 160 (2017) 1-10.

[21] Y. Xie, X. Liu, X. Ma, Y. Duan, Y. Yao, Q. Cai, Small Titanium-Based MOFs Prepared with the Introduction of Tetraethyl Orthosilicate and Their Potential for Use in Drug Delivery, ACS Appl Mater Interfaces, 10 (2018) 13325-13332.

[22] R.M. Abdelhameed, O.M. Darwesh, J. Rocha, A.M.S. Silva, IRMOF-3 Biological Activity Enhancement by Post-Synthetic Modification, Eur J Inorg Chem, 2019 (2019) 1243-1249.

[23] A. García Márquez, A. Demessence, A.E. Platero-Prats, D. Heurtaux, P. Horcajada, C. Serre, J.-S. Chang, G. Férey, V.A. de la Peña-O'Shea, C. Boissière, D. Grosso, C. Sanchez, Green Microwave Synthesis of MIL-100(Al, Cr, Fe) Nanoparticles for Thin-Film Elaboration, Eur. J. Inorg. Chem., 2012 (2012) 5165-5174.

[24] M. Giménez-Marqués, T. Hidalgo, C. Serre, P. Horcajada, Nanostructured metal–organic frameworks and their bio-related applications, Coord Chem Rev, 307 (2016) 342-360.

[25] V. Agostoni, P. Horcajada, V. Rodriguez-Ruiz, H. Willaime, P. Couvreur, C. Serre, R. Gref, 'Green' fluorine-free mesoporous iron(III) trimesate nanoparticles for drug delivery, Green Mater, 1 (2013) 209-217.

[26] T. Xue, C. Xu, Y. Wang, Y. Wang, H. Tian, Y. Zhang, Doxorubicin-loaded nanoscale metal–organic framework for tumor-targeting combined chemotherapy and chemodynamic therapy, Biomater Sci, 7 (2019) 4615-4623.

[27] W. Strzempek, E. Menaszek, B. Gil, Fe-MIL-100 as drug delivery system for asthma and chronic obstructive pulmonary disease treatment and diagnosis, Micropor Mesopor Mat, 280 (2019) 264-270.

[28] M.A. Simon, E. Anggraeni, F.E. Soetaredjo, S.P. Santoso, W. Irawaty, T.C. Thanh, S.B. Hartono, M. Yuliana, S. Ismadji, Hydrothermal Synthesize of HF-Free MIL-100(Fe) for Isoniazid-Drug Delivery, Sci Rep, 9 (2019) 16907.

[29] T. Hidalgo, M. Alonso-Nocelo, B.L. Bouzo, S. Reimondez-Troitiño, C. Abuin-Redondo, M. de la Fuente, P. Horcajada, Biocompatible iron(iii) carboxylate metal–organic frameworks as promising RNA nanocarriers, Nanoscale, 12 (2020) 4839-4845.

[30] T. Baati, L. Njim, F. Neffati, A. Kerkeni, M. Bouttemi, R. Gref, M.F. Najjar, A. Zakhama, P. Couvreur, C. Serre, P. Horcajada, In depth analysis of the in vivo toxicity of nanoparticles of porous iron(iii) metal-organic frameworks, Chem. Sci . 4 (2013) 1597-1607.

[31] T. Simon-Yarza, M. Giménez-Marqués, R. Mrimi, A. Mielcarek, R. Gref, P. Horcajada, C. Serre, P. Couvreur, A Smart Metal–Organic Framework Nanomaterial for Lung Targeting, Angew Chem Int Ed, 56 (2017) 15565-15569.

[32] T. Simon-Yarza, A. Mielcarek, P. Couvreur, C. Serre, Nanoparticles of Metal-Organic Frameworks: On the Road to In Vivo Efficacy in Biomedicine, Adv Mater, 30 (2018) 1707365.
[33] A. Lajevardi, M. Hossaini Sadr, M. Tavakkoli Yaraki, A. Badiei, M. Armaghan, A pH-responsive and magnetic Fe3O4@silica@MIL-100(Fe)/β-CD nanocomposite as a drug nanocarrier: loading and release study of cephalexin, New J. Chem., 42 (2018) 9690-9701.
[34] T. Azizi Vahed, M.R. Naimi-Jamal, L. Panahi, (Fe)MIL-100-Met@alginate: a hybrid polymer–MOF for enhancement of metformin's bioavailability and pH-controlled release, New J. Chem., 42 (2018) 11137-11146.
[35] S. Wuttke, S. Braig, T. Preiß, A. Zimpel, J. Sicklinger, C. Bellomo, J.O. Rädler, A.M. Vollmar, T. Bein, MOF nanoparticles coated by lipid bilayers and their uptake by cancer cells, Chem. Commun. (Cambridge, U. K.), 51 (2015) 15752-15755.
[36] M. Giménez-Marqués, E. Bellido, T. Berthelot, T. Simón-Yarza, T. Hidalgo, R. Simón-Vázquez, Á. González-Fernández, J. Avila, M.C. Asensio, R. Gref, P. Couvreur, C. Serre, P. Horcajada, GraftFast Surface Engineering to Improve MOF Nanoparticles Furtiveness, Small, 14 (2018) 1801900.
[37] T. Hidalgo, M. Giménez-Marqués, E. Bellido, J. Avila, M.C. Asensio, F. Salles, M.V. Lozano, M. Guillevic, R. Simón-Vázquez, A. González-Fernández, C. Serre, M.J. Alonso, P. Horcajada, Chitosan-coated mesoporous MIL-100(Fe) nanoparticles as improved bio-compatible oral nanocarriers, Sci Rep, 7 (2017) 43099.
[38] E. Bellido, T. Hidalgo, M.V. Lozano, M. Guillevic, R. Simón-Vázquez, M.J. Santander-Ortega, Á. González-Fernández, C. Serre, M.J. Alonso, P. Horcajada, Heparin-Engineered Mesoporous Iron Metal-Organic Framework Nanoparticles: Toward Stealth Drug Nanocarriers, Adv. Healthc. Mater., 4 (2015) 1246-1257.
[39] G. Cutrone, J. Qiu, M. Menendez-Miranda, J.M. Casas-Solvas, A. Aykaç, X. Li, D. Foulkes, B. Moreira-Alvarez, J.R. Encinar, C. Ladavière, D. Desmaële, A. Vargas-Berenguel, R. Gref, Comb-like dextran copolymers: A versatile strategy to coat highly porous MOF nanoparticles with a PEG shell, Carbohydr. Polym., 223 (2019) 115085.
[40] M. Řezanka, Monosubstituted Cyclodextrins as Precursors for Further Use, Eur. J. Org. Chem., (2016) 5322-5334.
[41] G. Crini, Review: A History of Cyclodextrins, Chem. Rev. (Washington, D. C.), 114 (2014) 10940-10975.
[42] A. Aykaç, M. Noiray, M. Malanga, V. Agostoni, J.M. Casas-Solvas, É. Fenyvesi, R. Gref, A. Vargas-Berenguel, A non-covalent “click chemistry” strategy to efficiently coat highly porous MOF nanoparticles with a stable polymeric shell, Biochim. Biophys. Acta., 1861 (2017) 1606-1616.
[43] V. Agostoni, P. Horcajada, M. Noiray, M. Malanga, A. Aykaç, L. Jicsinszky, A. Vargas-Berenguel, N. Semiramoth, S. Daoud-Mahammed, V. Nicolas, C. Martineau, F. Taulelle, J. Vigneron, A. Etcheberry, C. Serre, R. Gref, A “green” strategy to construct non-covalent, stable and bioactive coatings on porous MOF nanoparticles, Sci. Rep., 5 (2015) 7925.
[44] G. Cutrone, X. Li, J.M. Casas-Solvas, M. Menendez-Miranda, J. Qiu, G. Benkovics, D. Constantin, M. Malanga, B. Moreira-Alvarez, J.M. Costa-Fernandez, L. García-Fuentes, R. Gref, A. Vargas-Berenguel, Design of Engineered Cyclodextrin Derivatives for Spontaneous Coating of Highly Porous Metal-Organic Framework Nanoparticles in Aqueous Media, Nanomaterials, 9 (2019) 1103.
[45] V. Agostoni, T. Chalati, P. Horcajada, H. Willaime, R. Anand, N. Semiramoth, T. Baati, S. Hall, G. Maurin, H. Chacun, K. Bouchemal, C. Martineau, F. Taulelle, P. Couvreur, C. Rogez-Kreuz, P. Clayette, S. Monti, C. Serre, R. Gref, Towards an Improved anti-HIV Activity of NRTI via Metal–Organic Frameworks Nanoparticles, Avd. Helth. Mat., 2 (2013) 1630-1637.
[46] X. Li, L. Lachmanski, S. Safi, S. Sene, C. Serre, J.M. Grenèche, J. Zhang, R. Gref, New insights into the degradation mechanism of metal-organic frameworks drug carriers, Sci Rep, 7 (2017) 13142.
[47] J. Qiu, X. Li, K. Steenkeste, N. Barroca-Aubry, C. Aymes-Chodur, P. Roger, J.M. Casas-Solvas, A. Vargas-Berenguel, C. Rihouey, L. Picton, R. Gref, Self-assembled multifunctional core–shell highly porous metal–organic framework nanoparticles, Int.J Pharm, 581 (2020) 119281.
[48] W. Tang, S.-C. Ng, Facile synthesis of mono-6-amino-6-deoxy-α-, β-, γ-cyclodextrin hydrochlorides for molecular recognition, chiral separation and drug delivery, Nat Protoc, 3 (2008) 691-697.
[49] A. Perez-Anes, A. Szarpak-Jankowska, D. Jary, R. Auzély-Velty, β-CD-Functionalized Microdevice for Rapid Capture and Release of Bacteria, ACS Appl. Mater. Interfaces, 9 (2017) 13928-13938.
[50] A. Chucholowski, T. Hermann, B. Ayida, T. Wang, A. Khasanov, Cyclodextrin conjugates for SiRNA delivery, in: World Intellectual Property Organization, US, 2010, pp. 94.
[51] R. Wu, U.A. Jayasooriya, R.D. Cannon, Vibrational coupling in oxo-centred trinuclear clusters: oxygen-16/18 isotopic substitution studies of [FeIII3O(O2CC(CH3)3)6(py)3][FeCl4] and [FeIII2FeIIO(O2CC(CH3)3)6(py)3], Spectrochim Acta A Mol. Biomol. Spectrosc., 56 (2000) 575-579.
[52] A. Golmohamadpour, B. Bahramian, A. Shafiee, L. Ma’mani, Slow Released Delivery of Alendronate Using β-Cyclodextrine Modified Fe–MOF Encapsulated Porous Hydroxyapatite, J. Inorg. Organomet. P., 28 (2018) 1991-2000.
[53] X. Mao, Y. Lu, X. Zhang, Y. Huang, β-Cyclodextrin functionalization of metal-organic framework MOF-235 with excellent chemiluminescence activity for sensitive glucose biosensing, Talanta, 188 (2018) 161-167.
[54] G. Liu, L. Li, Y. Gao, M. Gao, X. Huang, J. Lv, D. Xu, A beta-cyclodextrin-functionalized magnetic metal organic framework for efficient extraction and determination of prochloraz and triazole fungicides in vegetables samples, Ecotoxicol. Environ. Saf., 183 (2019) 109546.
[55] S.D. Taherzade, J. Soleimannejad, A. Tarlani, Application of Metal-Organic Framework Nano-MIL-100(Fe) for Sustainable

Release of Doxycycline and Tetracycline, Nanomaterials, 7 (2017) 1-14.
[56] G. Chaturvedi, A. Kaur, A. Umar, M.A. Khan, H. Algarni, S.K. Kansal, Removal of fluoroquinolone drug, levofloxacin, from aqueous phase over iron based MOFs, MIL-100(Fe), J. Solid State Chem., 281 (2020) 121029.
[57] E. Bellido, M. Guillevic, T. Hidalgo, M.J. Santander-Ortega, C. Serre, P. Horcajada, Understanding the Colloidal Stability of the Mesoporous MIL-100(Fe) Nanoparticles in Physiological Media, Langmuir, 30 (2014) 5911-5920.
[58] J. Qiu, X. Li, K. Steenkeste, N. Barroca-Aubry, C. Aymes-Chodur, P. Roger, J.M. Casas-Solvas, A. Vargas-Berenguel, C. Rihouey, L. Picton, R. Gref, Self-assembled multifunctional core–shell highly porous metal–organic framework nanoparticles, Int. J. Pharm., 581 (2020) 119281.